Hypergraph Regularization-Based Anchor Learning for Multi-View Clustering

Yunpeng Zeng, Peng Song, Beihua Yang, Changjia Wang, Guanghao Du, Yanwei Yu, Wenming Zheng

PII: S0031-3203(25)01128-8
DOI: https://doi.org/10.1016/j.patcog.2025.112465
Reference: PR 112465

To appear in: *Pattern Recognition*

Received date: 1 June 2025
Revised date: 24 August 2025
Accepted date: 22 September 2025

Please cite this article as: Yunpeng Zeng, Peng Song, Beihua Yang, Changjia Wang, Guanghao Du, Yanwei Yu, Wenming Zheng, Hypergraph Regularization-Based Anchor Learning for Multi-View Clustering, *Pattern Recognition* (2025), doi: https://doi.org/10.1016/j.patcog.2025.112465

highlights

- A novel fast MVSC method is developed
- The higher-order correlations between anchor points is explored by hypergraph
- An orthogonal diversity constraint is utilized
- Experiments show that HRFAL has low time cost and good clustering performance

A novel fast MVSC method is developed 2. The higher-order correlations between anchor points is explored by hypergraph 3. An orthogonal diversity constraint is utilized 4. Experiments show that HRFAL has low time cost and good clustering performance

Hypergraph Regularization-Based Anchor Learning for Multi-View Clustering

Yunpeng Zeng[a], Peng Song[a,*], Beihua Yang[a], Changjia Wang[a], Guanghao Du[a], Yanwei Yu[b], Wenming Zheng[c]

[a]*School of Computer and Control Engineering, Yantai University, Yantai 264005, China*
[b]*College of Computer Science and Technology, Ocean University of China, Qingdao 266400, China*
[c]*Key Laboratory of Child Development and Learning Science (Ministry of Education), Southeast University, Nanjing 210096, China*

Abstract

Current anchor graph-based multi-view clustering methods can effectively address the problem of high computational cost for clustering large-scale multimedia data. However, they have the following shortcomings: (1) The relationships between anchor points are not adequately considered. (2) The correlations between the consistent anchor graph and diverse anchor graphs are ignored. To handle these issues, we propose a novel multi-view clustering method named Hypergraph Regularization-Based Anchor Learning (HRFAL). Specifically, we first process the original data to obtain a consistent anchor graph and diverse anchor graphs, which can explore more comprehensive consistent and complementary information. Meanwhile, the hyper-Laplacian regularization is applied to the anchor points to explore the higher-order relationships between the anchor points, thus enabling the generation of high-quality anchor graphs. Furthermore, the orthogonal diversity constraints are imposed on the consistent and diverse anchor graphs to enhance the distinction between the consistent and diverse components, resulting in better exploitation of consistent and complementary information. Finally, the Schatten p-norm constraint is implemented on the consistent anchor graph to maintain its low-rank structure, thus obtaining more robust consistent information. Experimental results on eight multi-view datasets show that HRFAL exhibits superior performance in terms of accuracy and speed.

Keywords: Anchor graph, hyper-Laplacian regularization, multi-view learning, Schatten p-norm

*Corresponding author
Email addresses: yunpengzeng@s.ytu.edu.cn (Yunpeng Zeng), pengsong@ytu.edu.cn (Peng Song), beihuayang@s.ytu.edu.cn (Beihua Yang), 202300358009@s.ytu.edu.cn (Changjia Wang), guanghaodu@s.ytu.edu.cn (Guanghao Du), yuyanwei@ouc.edu.cn (Yanwei Yu), wenming_zheng@seu.edu.cn (Wenming Zheng)

1. Introduction

With the advent of Internet era, a large amount of multi-dimensional data has been generated, which frequently manifests in a variety of forms [1, 2]. For example, an item can be photographed from different angles, a sentence can be expressed in multiple languages, and a brief video can encompass various forms of information, such as subtitles, video, and audio. Each of these disparate types of data possesses unique characteristics, and multi-view clustering (MVC) techniques facilitate the rapid and efficient fusion and analysis of these data [3]. In recent years, MVC and multiple labels have been used extensively in many applications [4], including document clustering [5], recommendation systems [6], and social network analysis [7].

Over the past decades, researchers have proposed a variety of MVC models. Among them, multi-view subspace clustering (MVSC) has become increasingly popular due to its good capacity to learn low-dimensional subspace representations [8, 9]. For example, Luo et al. [10] use a shared consistent representation and a set of specific representations to construct multi-view self-representation matrices. Zhang et al. [11] propose a consistent one-step subspace clustering method, which optimally fuses discriminative division-level information to eliminate noise between data. To simultaneously explore the consistent and diverse subspaces, Si et al. [12] factorize the subspace into consistent and diverse matrices, and utilize the obtained consistent and diverse matrices to learn the clustering labels. Zheng et al. [13] explore the higher-order information by imposing low-rank tensor constraints on multiple subspace representations. Wang et al. [14] develop a deep MVSC method that learns consensus self-representation from features obtained by adaptive fusion and structural supervision to generate high-quality pseudo-labels. In addition, the label distribution learning leverages label correlations to enhance learning performance, offering valuable insights for MVC methods [15, 16].

Despite the evident strengths of MVSC models in terms of clustering performance, there are still certain shortcomings. Existing MVSC models are computationally expensive, making them unsuitable for handling large-scale datasets. To address this problem, some anchor-based MVSC methods have been proposed. They construct the anchor graphs with size $m \times n$ between the anchor points and samples by employing m anchor points as representatives of n samples. Therefore, utilizing the obtained anchor graphs instead of the learned affinity graph with size $n \times n$ can effectively decrease the complexity of the actual operation. For instance, Lao et al. [17] propose a scalable MVC method based on multiple bipartite graphs, which jointly learns and fuses the bipartite graphs from multiple views. Zhang et al. [18] propose an anchor-based diverse anchor graph fusion method that uses a novel hybrid fusion strategy for multi-sized anchor graphs, which greatly reduces the time overhead. Ou et al. [19] combine the hierarchical

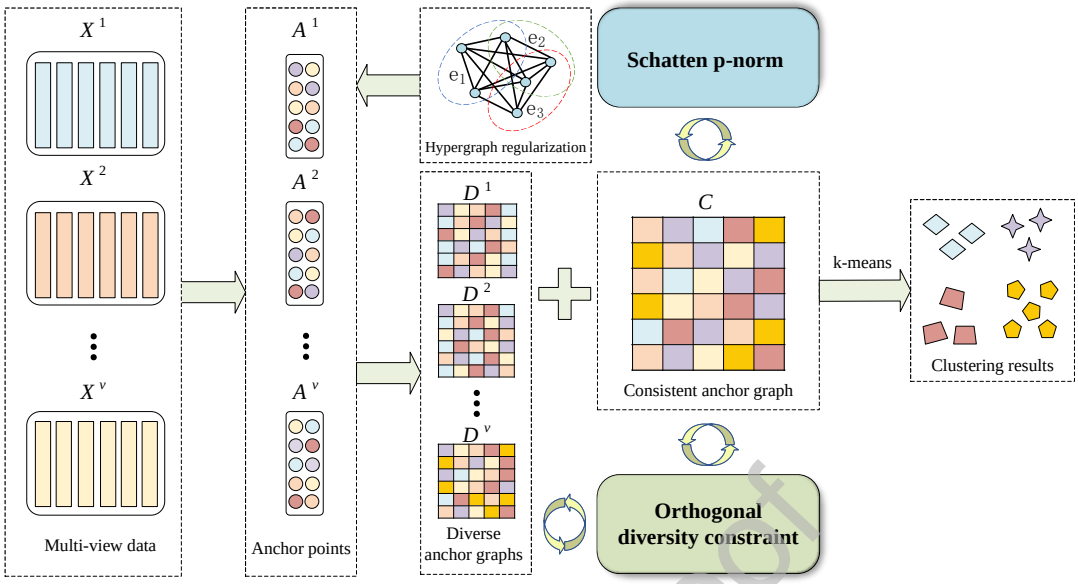

Fig. 1: The workflow of HRFAL. HRFAL learns the diverse anchor graphs D^v and a consistent anchor graph C from the original multi-view data, followed by the introduction of hyper-Laplacian regularization to explore the higher-order relationships between anchor points A^v. In addition, the orthogonal diversity constraint is introduced between the consistent anchor C and diverse anchor graphs D^v, and the Schatten p-norm constraint is imposed on the consistent anchor graph C. Finally, we utilize the consistent anchor graph C to obtain the final clustering results.

feature descent with anchor graph learning to cope with the differences between views. Wang et al. [20] develop a flexible anchor graph fusion framework to adaptively fuse multiple anchor graphs of different sizes using a novel structural alignment regularization. Liu et al. [21] use the relationship between anchor points and samples in different views to enhance the anchor points in the current view, thereby narrowing the spatial distribution of the anchor points. The anchor-based MVSC methods have achieved remarkable results. However, on one hand, they lack consideration of the relationships between anchor points. On the other hand, they ignore the orthogonal diversity of the consistent anchor graph and diverse anchor graphs.

To tackle the above-mentioned issues, we propose a novel anchor-based MVSC method called Hypergraph Regularization-Based Anchor Learning for multi-view clustering (HRFAL). Specifically, HRFAL employs hyper-Laplacian regularization on the anchor points, which explores the higher-order correlations between the anchor points and renders the learned anchor graphs more compact. Meanwhile, the distinctions between the consistent anchor graph and the diverse anchor graphs are maximized through the implementation of the orthogonal diversity constraint on them. Additionally, the Schatten p-norm con-

straint is imposed on the consistent anchor graph to obtain robust consistent information. The diagram of the proposed HRFAL model is shown in Fig. 1.

As a summary, the technical contributions of our method are concluded in the following three folds:

- HRFAL explores the higher-order correlations between anchor points and enhances the connections between them through the consistent hypergraph-induced hyper-Laplacian regularization of anchor points, which in turn enhances the learning quality of anchor graphs.
- We introduce an orthogonal diversity constraint to maximize the difference between the consistent anchor graph and the diverse anchor graphs, which guarantees their disparity construction. This effectively avoids the information loss and better exploits the consistent and complementary information.
- Extensive experiments show that HRFAL has low time cost and good clustering performance, which enables it to efficiently process large-scale datasets.

The structure of this paper is as follows. In Section 2, we present some popular MVSC methods. In Section 3, we introduce the proposed HRFAL method. Subsequently, the optimization process of the HRFAL model is elaborated. The experimental results are analyzed in Section 4. Finally, Section 5 summarizes this paper.

2. Related work

In this work, we focus on subspace-based clustering methods due to their flexibility and ability to handle high-dimensional data. We first review the subspace clustering methods and their extensions. Then, we introduce the anchor graph learning framework to address the problem of large-scale data.

2.1. Multi-view subspace clustering

The core idea of MVSC is to ascertain the optimal low-dimensional subspace representations under each view, and then integrate these representations through fusion strategies to obtain comprehensive and consistent clustering results. Given the multi-view data $X^v \in \mathbb{R}^{d^v \times n}$ with n samples of d^v dimensions in the v-th view, the framework of the self-representation clustering can be expressed as

$$\begin{aligned} &\min_{S^v} \sum_{v=1}^{V} \left\| X^v - X^v S^v \right\|_F^2 + \Psi(S^v) \\ &\text{s.t. } (S^v)^T \mathbf{1} = \mathbf{1}, S^v \geq 0 \end{aligned} \tag{1}$$

where S^v is the self-representation matrix, and $\Psi(\cdot)$ denotes various regularizations of S^v. The constraints on S^v ensure that the obtained self-representation matrices are non-negative and normalized.

In past studies, some researchers have devised various forms of $\Psi(\cdot)$ to deal with self-representation matrices [22]. For example, in [23], Wang et al. explore the complementary information between different self-representation matrices from different views by introducing an exclusivity term. In [24], Zheng et al. impose a bilinear factorization with orthogonality constraints and low-rank constraints on the self-representation matrices to exploit the consistent information of multi-view data. In [25], Li et al. construct a hypergraph using the uniform affinity matrix to preserve the higher-order relationships of incomplete data. In [26], Zhang et al. reduce the computational overhead of the solution by factorizing the view-specific self-representation matrices into two matrices. In [27], Peng et al. propose a hypergraph-based pairwise constraint propagation algorithm to construct an information similarity matrix, which effectively reveals higher-order relationships. In [28], Dong et al. perform self-representation learning on similar data matrices to alleviate the errors that occur when directly selecting original data for self-representation learning. However, when confronted with large-scale datasets, high computational costs, and space requirements, the applicability of self-representation clustering methods is hindered. Therefore, it is extremely important to reduce the computational cost.

2.2. Anchor based multi-view subspace clustering

In recent years, anchor-based MVSC models are rapidly developing due to their fast and efficient characteristics [29]. The core idea is to select a set of anchor points from the original samples and then construct a matrix of relationships between the anchor points and samples.

To apply the anchor strategy to multi-view graph clustering, we construct a relationship matrix between anchor points and samples on each view. Then, the anchor-based MVSC can be constructed, which is formulated as follows:

$$\begin{aligned} &\min_{A^v, Z^v} \sum_{v=1}^{V} \left\| X^v - A^v Z^v \right\|_F^2 + \Omega(Z^v) \\ &\text{s.t. } (Z^v)^T \mathbf{1} = \mathbf{1}, Z^v \geq 0 \end{aligned} \tag{2}$$

where $A^v \in \mathbb{R}^{d^v \times m}$ is an anchor points matrix composed of m selected anchor points, and Z^v is the anchor graph constructed from the anchor points. Note that the anchor graphs Z^v with size $m \times n$ can significantly reduce the time cost compared to the self-representation matrix S^v with size $n \times n$. Thus, the anchor-based MVSC methods are more applicable and efficient when dealing with large-scale data.

In the context of anchor-based MVSC, the important steps are how to select better anchor points and the processing of anchor graphs. Therefore, some related models are proposed. For instance, Xia et

al. [30] exploit the similarity of inter-view by applying the tensor Schatten p-norm, which more fully explores the spatial structure and complementary information embedded in the anchor graphs. Liu et al. [31] combine anchor learning and graph construction into a unified framework that directly outputs clustering labels by imposing a graph connectivity constraint. Zhang et al. [32] use denoised pixels and initial anchor points to perform both projection learning and structured anchor graphs learning in a one-step learning model to directly get the clustering results. Liu et al. [33] propose a robust and consistent anchor graph learning method, where the consistent anchor graph generated is used to capture the common structure between multiple views and filter out view-specific noise. Zhang et al. [34] enhance the clustering structure of potential anchors by learning different clustering centers to improve the differentiation of the subspace representation. Wu et al. [35] perform non-negative matrix factorization directly on the anchor graph to obtain the clustering labels, which improved the clustering efficiency.

Although the above methods offer a significant performance improvement, they could be further improved by considering the following aspects: (1) Existing methods lack consideration of the relationships between anchor points and thus fail to learn better anchor graphs. (2) The differences between consistent anchor graph and diverse anchor graphs are ignored, leading to underutilization of consistent and complementary information.

3. Proposed method

In this section, we first describe the symbols used in this paper. Then, we present the combinatorial modules of the proposed HRFAL, followed by the detailed optimization process. Finally, the analysis of the computational complexity is given.

3.1. Preliminary

In this paper, the matrices are represented by uppercase letters, e.g., $Q \in \mathbb{R}^{a\times b}$. For an arbitrary matrix Q, Q^{-1}, $\mathrm{Tr}(Q)$, and Q^T mean the inverse, trace, and transpose operations of Q, respectively. In addition, the Frobenius norm for Q is defined as $\|Q\|_F = \sqrt{\mathrm{Tr}(Q^TQ)} = \sqrt{\sum_{i=1}^{a}\sum_{j=1}^{b} g_{ij}^2}$, and $\|Q\|_{sp}^p$ represents the Schatten p-norm of Q. More symbols are listed in Table 1.

3.2. Consistent and diverse anchor graphs learning

In recent years, many anchor-based MVSC methods have been proposed to reduce the high computational complexity. However, most of them focus on the consistent anchor graphs, and fail to fully exploit the diverse information. To solve this problem, we construct both the consistent part of the anchor graphs

Table 1: Description of notations.

Notations	Meaning
$X^v \in \mathbb{R}^{d^v \times n}$	The data matrix of the v-th view
$A^v \in \mathbb{R}^{d^v \times m}$	The anchor matrix of the v-th view
$C \in \mathbb{R}^{m \times n}$	The consistent anchor graph for all views
$D^v \in \mathbb{R}^{m \times n}$	The diverse anchor graph of the v-th view
d^v	The feature dimensionality of the v-th view
I	The identity matrix
n	The number of samples
K	The number of clusters
V	The number of views
m	The number of anchor points
α, β, γ	The regularization parameters
$\left\|\cdot\right\|_{sp}^{p}$	The Schatten p-norm

and the diverse part of each view. Thus, we decompose the anchor graph Z^v into a consistent anchor graph C and diverse anchor graph D^v, which is formulated as

$$Z^v = C + D^v \tag{3}$$

Then, the consistent and diverse anchor graphs learning can be written in the following form:

$$\begin{aligned} &\min_{A^v, C, D^v} \sum_{v=1}^{V} \left\|X^v - A^v(C + D^v)\right\|_F^2 + \gamma \left\|C\right\|_* \\ &\text{s.t. } C \geq 0, C^T\mathbf{1} = \mathbf{1}, D^v \geq 0, (D^v)^T\mathbf{1} = \mathbf{1} \end{aligned} \tag{4}$$

where γ is the regularization parameter, and $\left\|\cdot\right\|_*$ denotes the nuclear norm that maintains the consistent anchor graph low-rank.

3.3. Anchor hypergraph regularization

Existing anchor-based MVC methods do not consider the relationships between anchor points, resulting in suboptimal learned anchor graphs. In particular, the hypergraph can accurately capture many-to-many and higher-order relationships in complex systems. Moreover, the consistent anchor graph C can capture the consensus information across all views and possesses a global structure, making the constructed hypergraph more representative. To this end, we construct a k-nearest neighbor (KNN) hypergraph based on the consistent anchor graph C. Then, the hyper-Laplacian regularization is employed

to explore the higher-order relationships of the anchor points. To better understand the definition of hypergraph regularization, we provide a brief introduction to the basic concepts involved.

Given a set of n vertices $U = \{u_i\}_{i=1}^{n}$, $E = \{e_j\}_{j=1}^{t}$ is the set of the hyperedges e_j, and $W = \mathrm{diag}\{w(e_1), w(e_2), \ldots, w(e_t)\}$ is the weight matrix associated with the hyperedges e_j [36]. Unlike the graph, the hypergraph allows a hyperedge to connect any number of vertices. Given a hypergraph $G = (U, E, W)$, each vertex and its K-nearest neighbors are formulated as a hyperedge, in which the relationships between vertices and hyperedges are represented by the association matrix $H \in \mathbb{R}^{|U|\times|E|}$, which is defined as

$$h(u_i, e_j) = \begin{cases} S_{ij}, & \text{if } u_i \in e_j \\ 0, & \text{otherwise} \end{cases} \tag{5}$$

where $S \in \mathbb{R}^{|U|\times|U|}$ is the affinity matrix constructed via KNN.

Then, we compute the degree of vertices $u_i \in U$ and hyperedges $e_j \in E$ by

$$\begin{aligned} d(u_i) &= \sum_{e_j \in E} w(e_j) h(u_i, e_j) \\ d(e_j) &= \sum_{v_i \in U} h(u_i, e_j) \end{aligned} \tag{6}$$

where $d(u_i)$ and $d(e_j)$ are the elements corresponding to the two diagonal matrices D_U and D_E, respectively. Finally, the hyper-Laplacian matrix [37] is defined as

$$L_h = D_U - H\mathbf{W}D_E^{-1}H^T \tag{7}$$

Furthermore, the hyper-Laplacian regularization of the anchor points can be formulated in the following form:

$$\min_{A^v} \sum_{v=1}^{V} Tr(A^v L_h (A^v)^T) \tag{8}$$

3.4. Orthogonal diversity constraint

To learn more representative consistent anchor graph C, we introduce an orthogonal diversity constraint to maximize the difference between consistent and diverse anchor graphs. This guarantees the disparity construction of the consistent anchor graph and the diverse anchor graphs, while enhancing the ability to explore complementary information. The orthogonal diversity constraint can be formulated as follows:

$$\begin{aligned} &\min_{C, D^v} \sum_{v=1}^{V} \left\| C^T D^v \right\|_F^2 \\ &\text{s.t. } C \geq 0, C^T\mathbf{1} = \mathbf{1}, D^v \geq 0, (D^v)^T\mathbf{1} = \mathbf{1} \end{aligned} \tag{9}$$

where C and D^v are the previously obtained anchor graphs for the consistent and diverse parts, respectively.

3.5. Schatten p-norm constraint

The nuclear norm and the Schatten p-norm are common functions used to maintain the low-rank nature of matrices. According to previous studies [38], the Schatten p-norm can yield better performance than the nuclear norm. Thus, in our study, the Schatten p-norm is utilized to maintain the low-rank property of the consistent anchor graph C, which is defined as follows:

$$\left\|C\right\|_{sp}^{p} = \sum_{t=1}^{\min(m,n)} \theta_i^p \tag{10}$$

where θ_i is the i-th largest singular value of C. Note that when $p = 1$ or 2, the Schatten p-norm is equivalent to the nuclear norm or the Frobenius norm, respectively.

3.6. Overall objective function

By combining the consistent and diverse anchor graphs learning in Eq. (4), the hypergraph regularization in Eq. (8), the orthogonal diversity constraint in Eq. (9), and the Schatten p-norm constraint (10), we can formulate the objective function of HRFAL by

$$\begin{aligned} \min_{A^v,C,D^v} & \sum_{v=1}^{V} \left\|X^v - A^v(C + D^v)\right\|_F^2 + \alpha \sum_{v=1}^{V} Tr(A^v L_h (A^v)^T) \\ & + \beta \sum_{v=1}^{V} \left\|C^T D^v\right\|_F^2 + \gamma \left\|C\right\|_{sp}^{p} \\ \text{s.t. } & C \geq 0, C^T \mathbf{1} = \mathbf{1}, D^v \geq 0, (D^v)^T \mathbf{1} = \mathbf{1} \end{aligned} \tag{11}$$

where α, β, and γ are the regularization parameters.

3.7. Optimization

To optimize Eq. (11), we use an alternating iteration method. During the optimization process, we introduce an intermediate variable $C = Z$. The objective function can be reformulated in the following form:

$$\begin{aligned} \min_{A^v,C,D^v} & \sum_{v=1}^{V} \left\|X^v - A^v(C + D^v)\right\|_F^2 + \alpha \sum_{v=1}^{V} Tr(A^v L_h (A^v)^T) \\ & + \beta \sum_{v=1}^{V} \left\|C^T D^v\right\|_F^2 + \gamma \left\|Z\right\|_{sp}^{p} \\ \text{s.t. } & C \geq 0, C^T \mathbf{1} = \mathbf{1}, D^v \geq 0, (D^v)^T \mathbf{1} = \mathbf{1}, C = Z \end{aligned} \tag{12}$$

The Lagrangian function corresponding to Eq. (12) can be expressed as

$$\begin{aligned}\min_{A^v,C,D^v} &\sum_{v=1}^{V}\left\|X^v - A^v(C+D^v)\right\|_F^2 + \alpha\sum_{v=1}^{V} Tr(A^v L_h (A^v)^T) \\ &+ \beta\sum_{v=1}^{V}\left\|C^T D^v\right\|_F^2 + \gamma\left\|Z\right\|_{sp}^p + \frac{\mu}{2}\left\|C - Z + \frac{Y}{\mu}\right\|_F^2 \\ \text{s.t. } & C \geq 0, C^T\mathbf{1} = \mathbf{1}, D^v \geq 0, (D^v)^T\mathbf{1} = \mathbf{1}\end{aligned} \tag{13}$$

where μ is the trade-off parameter, and Y is the Lagrangian multiplier. Then the optimization problem for Eq. (13) is divided into five sub-problems.

(1) Update A^v: Fix C and D^v to update A^v. The optimization of A^v can be written as

$$\min_{A^v}\mathcal{L}(A^v) = \left\|X^v - A^v(C+D^v)\right\|_F^2 + \alpha Tr(A^v L_h (A^v)^T) \tag{14}$$

In particular, the matrix A^v in each view may be updated respectively. Then, the partial derivative of A^v is obtained as

$$\frac{\partial\mathcal{L}(A^v)}{\partial A^v} = -2(X^v - A^v(C+D^v))(C+D^v)^T + 2\alpha A^v L_h \tag{15}$$

By setting $\frac{\partial\mathcal{L}(A^v)}{\partial A^v} = 0$, we have

$$A^v = \{X^v(C+D^v)^T\}\{(C+D^v)(C+D^v)^T + \alpha L_h\}^{-1} \tag{16}$$

(2) Update C: Fix A^v, D^v, and Z to update C, we have

$$\begin{aligned}\min_{C}\mathcal{L}(C) = &\sum_{v=1}^{V}\left\|X^v - A^v(C+D^v)\right\|_F^2 + \beta\sum_{v=1}^{V}\left\|C^T D^v\right\|_F^2 \\ &+ \frac{\mu}{2}\left\|C - Z + \frac{Y}{\mu}\right\|_F^2 \\ \text{s.t. } & C \geq 0, C^T\mathbf{1} = \mathbf{1}\end{aligned} \tag{17}$$

Then, calculate the partial derivative of C, we get

$$\begin{aligned}\frac{\partial\mathcal{L}(C)}{\partial C} = &\sum_{v=1}^{V} 2\beta D^v (D^v)^T C - \sum_{v=1}^{V} 2(A^v)^T(X^v - A^v(C+D^v)) \\ &+ \mu(C - Z + \frac{Y}{\mu})\end{aligned} \tag{18}$$

By setting $\frac{\partial\mathcal{L}(C)}{\partial C} = 0$, we get

$$\begin{aligned}C = (&\sum_{v=1}^{V} 2(A^v)^T A^v + \sum_{v=1}^{V} 2\beta D^v (D^v)^T + \mu I)^{-1}(\sum_{v=1}^{V} 2(A^v)^T X^v \\ &- \sum_{v=1}^{V} 2(A^v)^T A^v D^v + \mu Z - Y)\end{aligned} \tag{19}$$

(3) Update D^v: Fix A^v and C to update D^v. The optimization of D^v can be rewritten as follows:

$$\begin{aligned} &\min_{D^v} \mathcal{L}(D^v) = \left\|X^v - A^v(C + D^v)\right\|_F^2 + \beta\left\|C^T D^v\right\|_F^2 \\ &\text{s.t. } D^v \geq 0, (D^v)^T \mathbf{1} = \mathbf{1} \end{aligned} \tag{20}$$

Similar to the optimization of C, the partial derivative of D^v is written as

$$\frac{\partial \mathcal{L}(D^v)}{\partial D^v} = -2(A^v)^T(X^v - A^v(C + D^v)) + 2\beta CC^T D^v \tag{21}$$

By setting $\frac{\partial \mathcal{L}(D^v)}{\partial D^v} = 0$, we have

$$D^v = ((A^v)^T A^v + \beta CC^T)^{-1}((A^v)^T X^v - (A^v)^T A^v C) \tag{22}$$

(4) Update Z: Update Z by fixing C, the update of Z can be written as follows:

$$\begin{aligned} &\min_{Z} \mathcal{L}(Z) = \gamma\left\|Z\right\|_{sp}^p + \frac{\mu}{2}\left\|Z - C - \frac{Y}{\mu}\right\|_F^2 \\ &\text{s.t. } C \geq 0, C^T \mathbf{1} = \mathbf{1} \end{aligned} \tag{23}$$

Eq. (23) is equivalent to

$$\min_{Z} \eta\left\|Z\right\|_{sp}^p + \frac{1}{2}\left\|Z - R\right\|_F^2 \tag{24}$$

where $R = C + \frac{Y}{\mu}$ and $\eta = \frac{\gamma}{\mu}$.

To update Z, the optimal solution is $M\Delta N^T$, where $\Delta = \text{diag}(\theta_1, \ldots, \theta_l)$, and θ_i is obtained by

$$\min_{\theta_i} \frac{1}{2}(\theta_i - \varrho_i)^2 + \eta\theta_i^p \tag{25}$$

where ϱ_i is the i-th singular value of R. To solve problem (25), we use the generalized soft-thresholding algorithm [39]. Algorithm 1 details the process of updating the variable Z.

(5) Update Y: Y and μ are updated as follows:

$$Y = Y + \mu(C - Z) \tag{26}$$

$$\mu = \min(\mu_{\max}, \omega\mu) \tag{27}$$

where ω is a constant.

For ease of understanding, we summarize the above optimization procedures in Algorithm 2.

3.8. Complexity analysis

Based on the optimization procedures in Algorithm 2, we analyze the time complexity of HRFAL. For updating A^v and D^v, the inverse of the matrix needs to be resolved, which has the time complexity of $O(nmdV)$ and $O(m^2nV)$, where $d = \sum_{v=1}^{V} d^v$, and V is the number of views. Updating the consistent anchor graph C requires the time complexity of $O(m^2n)$. We use the SVD operator to update Z, thus the time complexity of this step is $O(mn)$. In a nutshell, the complexity of HRFAL is $O((nmdV + m^2n + m^2nV + mn)t)$, where t is the number of iterations.

Algorithm 1 $\min_{Z} \eta \|Z\|_{sp}^{p} + \frac{1}{2}\|Z - R\|_{F}^{2}$

Input: R, p, and η

Singular value decomposition $R = M\varphi N^{T}$, $\varphi = \mathrm{diag}(\varrho_1, \ldots, \varrho_l)$.

for $t = 1 : l$ **do**

$\tau_p^{GST}(\gamma) = (2\gamma(1-p))^{\frac{1}{2-p}} + \gamma p(2\gamma(1-p))^{\frac{p-1}{2-p}}$.

if $\varrho_i < \tau_p^{GST}$ **then**

$\theta_i = 0$.

else

$\theta_i^r = \varrho_i$.

for $r = 0, 1, 2$ **do**

$\theta_i^{r+1} = \varrho_i - \gamma p(\theta_i^{(r)})^{p-1}$.

$r = r + 1$.

end

end

end

$\Delta = \mathrm{diag}(\theta_1 \ldots, \theta_l)$.

Output: $Z = M\Delta N^{T}$

4. Experiments

In this section, we conduct comprehensive experiments by comparing HRFAL with eight popular methods on eight real-world datasets. The experiments are performed on a Windows PC with an Intel Core i7-12700KF 3.6 GHz CPU and 32 GB RAM. Note that we obtain the codes of all the compared methods from the authors' open-source GitHub repositories and rerun them using the same device configuration as HRFAL.

4.1. Datasets

We use eight popular benchmark datasets, including NGs [40], UCI [41], BDGP [33], Notting-Hill [8], Fashion [42], YTF10 [43], YTF20 [20], and YTF50 [44]. The corresponding information for these datasets is shown in Table 2, and the detailed description of these datasets is shown below.

- **NGs [40]:** The NGs is a text dataset containing 500 samples with three views.
- **UCI [41]:** The UCI comprises handwritten digital images containing a total of 2000 samples in ten

Algorithm 2 HRFAL

Input: The original multi-view datasets $\{X^1, \ldots, X^v\}$, the number of anchor points m, the number of clusters K, and regularization parameters α, β, γ, and p.

Initialize: $\forall v$, $A^v = D^v = 0$, $C = Z = Y$, $\mu = 1$, $\mu_{max} = 10^6$, and $\omega = 1.5$.

repeat

for $v = 1 : V$ **do**

Update A^v by Eq. (16).

end

Update C by Eq. (19).

for $v = 1 : V$ **do**

Update D^v by Eq. (22).

end

Update Z by Algorithm1.

Update Y by Eq. (26).

Update μ by Eq. (27).

Check the convergence conditions $\|C - Z\|_\infty < \epsilon$.

until convergence.

Perform k-means clustering on the consistent matrix C

Output: The clustering results with K clusters.

classes. Each image is characterized by three different features, namely, Fourier coefficients, pixel averages, and morphological features.

- **BDGP [33]:** The BDGP contains 2500 images of Drosophila embryos collected from three different views: lateral, dorsal, and ventral.
- **Notting-Hill [8]:** The Notting-Hill is a composition of face photos extracted from the film “Notting-Hill", which contains a total of 4660 photos.
- **Fashion [42]:** The Fashion is similar to the MNIST Handwritten Digits dataset, and comprises 10000 photos of clothing, categorized into ten groups.
- **YTF10 [43]:** The YTF10 consists of a subset of the YouTube face database. It has four distinct views, i.e., LBP, global information, histogram of oriented gradients, and texture.
- **YTF20 [20]:** As YTF10, the YTF20 contains richer face information from the YouTube database,

with 325 videos involving 1595 subjects and a total of 63896 face images.

- **YTF50 [44]:** The YTF50 has richer face information compared to YTF10 and YTF20. It has 50 categories and 126054 samples.

Table 2: Datasets description.

Datasets	#Instances	#Views	#Classes	#Features
NGs	500	3	5	2000 2000 2000
UCI	2000	3	10	240 76 6
BDGP	2500	3	5	100 500 250
Notting-Hill	4660	3	5	6750 3304 2000
Fashion	10000	3	10	784 784 784
YTF10	38654	4	10	944 576 512 640
YTF20	63896	4	20	944 576 512 640
YTF50	126054	4	50	944 576 512 640

4.2. Compared methods

To validate the superiority of our HRFAL model, we benchmark it against eight popular methods, including k-means [45], FDAGF [18], Orth-NTF [46], MVSC-HFD [19], OMVCDR [47], AEVC [21], ETEAL [48], and S^{2}BGFMC [35]. The details of the above methods are as follows:

- **k-means [45]:** k-means is applied to each view and the best results are chosen.
- **FDAGF [18]:** FDAGF is a diverse anchor graphs fusion method. The model is designed to learn the anchor graphs of different sizes in each view and uses a fusion strategy of different-sized anchor graphs to reduce the time overhead.
- **Orth-NTF [46]:** Orth-NTF executes matrix factorization on a tensor, which directly takes into account the relations between the views and utilizes the tensor Schatten p-norm constraint as a rank approximation to the third-order tensor.
- **MVSC-HFD [19]:** MVSC-HFD is an anchor-based MVSC model that combines hierarchical feature descent with anchor graph learning to deal with the differences between multiple views, revealing the dependencies between different views.

- **OMVCDR [47]:** OMVCDR projects all views to the latent space to learn global information and performs automatic weighted fusion, then obtains consistent discrete clustering labels in a one-step learning model.
- **AEVC [21]:** AEVC constructs views based on aligned initial anchor graphs to explore inter-view correlations. It utilizes the relationships between anchor points and samples on neighboring views to augment anchor points on the current view, thus narrowing the spatial distribution of anchor points on similar views.
- **ETEAL [48]:** ETEAL eliminates noise and redundant data in the original space by projecting the original data into the embedding space and learning the anchor graphs. Meanwhile, an augmented tensor strategy is used to recover the low-order properties of the embedded anchor graph.
- **S^{2}BGFMC [35]:** S^{2}BGFMC proposes the concept of anchor graphs factorization, where the NMF is performed directly on the anchor graphs to maintain the efficiency of the entire clustering process.

4.3. Performance analysis

To validate the superiority of HRFAL, we use ACC (Accuracy), NMI (Normalized mutual information), PUR (Purity), F-score, PRE (Precision), ARI (Adjusted rand index), and REC (Recall) as the evaluation metrics. Among them, ACC is used to assess the accuracy of the method for clustering. NMI is used to evaluate the similarity between the final clustering results and the real labels. PUR assesses the degree of match between clustering results and true labels. F-score is used to assess the comprehensive performance of the model. PER is used to measure the accuracy of the model prediction results. ARI is used to measure mainly similarity. REC is used to measure the model ability to cover the positive classes in the clustering task. For all the compared methods, the parameters are adjusted within a predefined threshold range, after which the clustering results for each dataset are recorded. The comparison results are shown in Tables 3 and 4, while the running time and time complexity are shown in Table 5. For each dataset, the most optimal results are indicated in bold, the second-best ones are denoted by underlining, and 'N/A' represents the memory overflow. From these tables, the following conclusions can be deduced:

- Note that for the advanced anchor-based MVC methods (MVSC-HFD, AEVC, ETEAL, and SBGFMC), they all learn anchor graphs directly or use pre-constructed anchor graphs, and then process them in a subsequent process. In contrast, HRFAL explores the relationships between anchor points through the consistent hypergraph-induced hyper-Laplacian regularization, which can enhance the quality of the anchor graph learning. Unlike MVSC-HFD and AEVC, which use a

Table 3: Comparison results on NGs, UCI, BDGP, and Notting-Hill.

Datasets	Methods	ACC(%)	NMI(%)	PUR(%)	F-score(%)	PRE(%)	ARI(%)	REC(%)
NGs	*k*-means	63.14(±6.35)	11.16(±4.05)	64.20(±5.07)	47.47(±4.35)	43.87(±5.66)	32.51(±6.23)	53.71(±4.52)
	FDAGF	67.00(±0.00)	46.15(±0.00)	72.80(±0.00)	51.27(±0.00)	58.46(±0.00)	37.13(±0.00)	45.66(±0.00)
	Orth-NTF	73.40(±0.00)	64.21(±0.00)	74.00(±0.00)	59.92(±0.00)	56.10(±0.00)	49.14(±0.00)	64.29(±0.00)
	MVSC-HFD	73.60(±0.00)	50.11(±0.00)	73.60(±0.00)	57.21(±0.00)	55.17(±0.00)	46.13(±0.00)	62.81(±0.00)
	OMVCDR	33.20(±0.00)	11.75(±0.00)	34.20(±0.00)	34.60(±0.00)	23.31(±0.00)	07.34(±0.00)	67.78(±0.00)
	AEVC	63.72(±1.69)	46.52(±0.81)	63.93(±0.86)	50.11(±0.85)	45.08(±0.99)	35.99(±1.10)	56.44(±1.74)
	ETEAL	80.00(±0.00)	63.81(±0.00)	80.00(±0.00)	67.96(±0.00)	68.38(±0.00)	59.97(±0.00)	67.54(±0.00)
	S^2BGFMC	77.20(±1.67)	52.64(±0.97)	77.20(±1.21)	61.57(±1.03)	61.31(±0.86)	52.01(±1.63)	61.83(±1.03)
	HRFAL	**98.60(±0.00)**	**95.47(±0.00)**	**98.60(±0.00)**	**97.19(±0.00)**	**97.22(±0.00)**	**97.22(±0.00)**	**97.17(±0.00)**
UCI	*k*-means	74.33(±0.82)	74.11(±0.63)	78.73(±0.69)	69.64(±0.91)	66.14(±0.79)	66.09(±1.01)	73.53(±1.05)
	FDAGF	86.70(±0.00)	80.12(±0.00)	86.75(±0.00)	77.59(±0.00)	78.58(±0.00)	75.08(±0.00)	76.63(±0.00)
	Orth-NTF	80.50(±0.00)	78.07(±0.00)	80.50(±0.00)	68.70(±0.00)	67.48(±0.00)	65.17(±0.00)	69.96(±0.00)
	MVSC-HFD	56.10(±0.00)	62.06(±0.00)	58.45(±0.00)	50.17(±0.00)	39.42(±0.00)	42.95(±0.00)	70.44(±0.00)
	OMVCDR	43.75(±0.00)	46.46(±0.00)	48.70(±0.00)	39.10(±0.00)	37.12(±0.00)	31.96(±0.00)	41.29(±0.00)
	AEVC	88.05(±3.36)	81.47(±1.95)	88.58(±3.20)	80.23(±3.63)	79.27(±4.47)	78.01(±4.08)	81.28(±2.87)
	ETEAL	84.60(±0.00)	76.12(±0.00)	84.60(±0.00)	74.08(±0.00)	74.54(±0.00)	71.20(±0.00)	73.63(±0.00)
	S^2BGFMC	82.50(±0.08)	73.60(±0.13)	82.50(±0.06)	70.65(±0.23)	70.24(±0.07)	67.39(±0.26)	71.07(±0.16)
	HRFAL	**92.35(±0.00)**	**84.83(±0.00)**	**92.35(±0.00)**	**85.50(±0.00)**	**85.73(±0.00)**	**83.89(±0.00)**	**85.26(±0.00)**
BDGP	*k*-means	44.37(±0.42)	27.96(±0.29)	47.79(±0.51)	38.78(±0.47)	37.22(±0.69)	22.69(±0.61)	40.50(±1.00)
	FDAGF	46.72(±0.00)	27.45(±0.00)	50.36(±0.00)	38.41(±0.00)	38.59(±0.00)	22.95(±0.00)	38.23(±0.00)
	Orth-NTF	55.56(±0.00)	**45.70(±0.00)**	57.48(±0.00)	48.23(±0.00)	46.51(±0.00)	34.71(±0.00)	50.08(±0.00)
	MVSC-HFD	41.60(±0.00)	15.84(±0.00)	41.60(±0.00)	31.24(±0.00)	26.73(±0.00)	10.21(±0.00)	43.15(±0.00)
	OMVCDR	56.96(±0.00)	35.58(±0.00)	59.36(±0.00)	46.10(±0.00)	44.47(±0.00)	32.03(±0.00)	47.85(±0.00)
	AEVC	60.64(±0.62)	30.88(±0.66)	60.64(±0.62)	43.38(±0.55)	43.24(±0.60)	29.20(±0.72)	43.53(±0.50)
	ETEAL	51.60(±0.00)	27.42(±0.00)	55.72(±0.00)	39.16(±0.00)	39.83(±0.00)	23.66(±0.00)	38.51(±0.00)
	S^2BGFMC	50.56(±1.31)	32.17(±2.45)	51.60(±1.96)	43.50(±1.36)	42.63(±1.45)	29.05(±2.51)	44.41(±1.63)
	HRFAL	**64.36(±0.00)**	44.22(±0.00)	**64.36(±0.00)**	**48.87(±0.00)**	**47.34(±0.00)**	**35.23(±0.00)**	**51.70**(±0.00)
Notting-Hill	*k*-means	84.71(±7.70)	74.59(±5.82)	86.21(±4.56)	78.49(±7.40)	78.64(±5.97)	72.51(±9.29)	78.42(±8.85)
	FDAGF	84.48(±0.00)	80.51(±0.00)	89.33(±0.00)	83.82(±0.00)	85.33(±0.00)	79.61(±0.00)	82.36(±0.00)
	Orth-NTF	59.09(±0.00)	47.92(±0.00)	60.45(±0.00)	47.07(±0.00)	48.53(±0.00)	32.74(±0.00)	45.69(±0.00)
	MVSC-HFD	87.44(±0.00)	77.46(±0.00)	87.44(±0.00)	81.36(±0.00)	80.06(±0.00)	76.01(±0.00)	82.70(±0.00)
	OMVCDR	90.66(±0.00)	81.54(±0.00)	81.54(±0.00)	86.48(±0.00)	87.72(±0.00)	81.54(±0.00)	87.23(±0.00)
	AEVC	86.38(±4.01)	74.49(±1.86)	86.94(±1.54)	78.10(±2.63)	76.10(±2.05)	71.73(±3.29)	80.22(±3.27)
	ETEAL	90.34(±0.00)	79.48(±0.00)	90.34(±0.00)	86.43(±0.00)	85.43(±0.00)	82.67(±0.00)	87.46(±0.00)
	S^2BGFMC	82.03(±0.25)	68.99(±0.31)	82.03(±0.36)	77.59(±0.17)	77.84(±0.31)	71.31(±0.32)	77.35(±0.23)
	HRFAL	**93.43(±0.00)**	**86.80(±0.00)**	**93.43(±0.00)**	**90.54(±0.00)**	**89.52(±0.00)**	**87.92(±0.00)**	**91.60(±0.00)**

Table 4: Comparison results on Fashion, YTF10, YTF20 and YTF50.

Datasets	Methods	ACC(%)	NMI(%)	PUR(%)	F-score(%)	PRE(%)	ARI(%)	REC(%)
Fashion	*k*-means	58.37(±1.45)	61.13(±1.03)	62.41(±1.67)	50.14(±1.62)	52.47(±1.95)	44.34(±1.77)	48.02(±1.34)
	FDAGF	69.20(±0.00)	68.96(±0.00)	74.82(±0.00)	60.99(±0.00)	65.80(±0.00)	56.31(±0.00)	56.84(±0.00)
	Orth-NTF	24.92(±0.00)	12.32(±0.00)	26.81(±0.00)	16.14(±0.00)	16.71(±0.00)	6.48(±0.00)	15.61(±0.00)
	MVSC-HFD	73.72(±0.00)	74.17(±0.00)	73.93(±0.00)	67.73(±0.00)	61.68(±0.00)	63.73(±0.00)	76.42(±0.00)
	OMVCDR	75.32(±0.00)	74.78(±0.00)	80.20(±0.00)	68.75(±0.00)	71.93(±0.00)	65.11(±0.00)	65.84(±0.00)
	AEVC	77.91(±1.63)	70.07(±0.55)	78.85(±1.13)	67.89(±1.15)	67.37(±1.67)	64.30(±1.31)	68.44(±0.69)
	ETEAL	62.34(±0.00)	66.37(±0.00)	69.15(±0.00)	56.87(±0.00)	60.35(±0.00)	51.77(±0.00)	53.77(±0.00)
	S^2BGFMC	79.03(±0.15)	71.90(±0.09)	79.03(±0.23)	69.86(±0.17)	70.20(±0.29)	66.49(±0.18)	69.51(±0.31)
	HRFAL	**83.30(±0.00)**	**80.94(±0.00)**	**84.37(±0.00)**	**77.33(±0.00)**	**77.82(±0.00)**	**74.80(±0.00)**	**76.85(±0.00)**
YTF10	*k*-means	72.03(±4.03)	75.14(±2.29)	76.70(±3.24)	67.80(±3.76)	69.15(±3.13)	63.76(±4.28)	66.52(±4.40)
	FDAGF	80.46(±0.00)	82.91(±0.00)	85.98(±0.00)	77.77(±0.00)	78.71(±0.00)	75.01(±0.00)	76.86(±0.00)
	Orth-NTF	N/A	N/A	N/A	N/A	N/A	N/A	N/A
	MVSC-HFD	82.10(±0.00)	81.41(±0.00)	82.10(±0.00)	74.41(±0.00)	75.82(±0.00)	71.31(±0.00)	74.57(±0.00)
	OMVCDR	73.82(±0.00)	75.11(±0.00)	74.22(±0.00)	66.79(±0.00)	66.86(±0.00)	62.72(±0.00)	66.72(±0.00)
	AEVC	79.03(±3.75)	82.38(±2.26)	84.20(±2.74)	76.51(±3.27)	76.04(±4.18)	73.60(±3.76)	77.03(±2.53)
	ETEAL	81.08(±0.00)	78.07(±0.00)	81.38(±0.00)	69.06(±0.00)	75.00(±0.00)	64.93(±0.00)	63.99(±0.00)
	S^2BGFMC	80.35(±0.67)	80.45(±0.54)	82.56(±0.76)	72.22(±0.54)	70.37(±0.81)	68.71(±0.36)	74.17(±0.61)
	HRFAL	**88.67(±0.00)**	**86.16(±0.00)**	**88.67(±0.00)**	**79.47(±0.00)**	**81.68(±0.00)**	**76.87(±0.00)**	**77.36(±0.00)**
YTF20	*k*-means	68.76(±2.71)	77.98(±0.51)	76.29(±0.92)	61.56(±2.24)	65.98(±1.95)	59.14(±2.44)	57.83(±3.80)
	FDAGF	73.89(±0.00)	81.20(±0.00)	79.73(±0.00)	61.28(±0.00)	71.58(±0.00)	58.65(±0.00)	53.57(±0.00)
	Orth-NTF	N/A	N/A	N/A	N/A	N/A	N/A	N/A
	MVSC-HFD	73.46(±0.00)	77.99(±0.00)	76.06(±0.00)	64.04(±0.00)	63.10(±0.00)	61.85(±0.00)	**71.76(±0.00)**
	OMVCDR	50.44(±0.00)	69.32(±0.00)	63.82(±0.00)	48.70(±0.00)	42.41(±0.00)	45.20(±0.00)	57.18(±0.00)
	AEVC	71.57(±4.01)	77.33(±1.45)	76.61(±2.10)	65.12(±2.13)	62.66(±4.26)	62.98(±1.23)	67.94(±1.31)
	ETEAL	68.83(±0.00)	79.00(±0.00)	78.11(±0.00)	59.65(±0.00)	68.44(±0.00)	56.95(±0.00)	52.85(±0.00)
	S^2BGFMC	N/A	N/A	N/A	N/A	N/A	N/A	N/A
	HRFAL	**78.11(±0.00)**	**79.43(±0.00)**	**81.30(±0.00)**	**67.80(±0.00)**	**71.53(±0.00)**	**65.80(±0.00)**	69.45(±0.00)
YTF50	*k*-means	68.40(±1.50)	81.60(±0.77)	75.66(±1.31)	61.50(±2.71)	64.83(±2.25)	60.57(±2.78)	58.53(±3.34)
	FDAGF	68.11(±0.00)	82.26(±0.00)	77.30(±0.00)	51.95(±0.00)	66.56(±0.00)	50.52(±0.00)	40.16(±0.00)
	Orth-NTF	N/A	N/A	N/A	N/A	N/A	N/A	N/A
	MVSC-HFD	68.98(±0.00)	82.25(±0.00)	72.03(±0.00)	62.85(±0.00)	59.11(±0.00)	61.33(±0.00)	**66.57(±0.00)**
	OMVCDR	71.83(±0.00)	81.94(±0.00)	77.32(±0.00)	63.10(±0.00)	67.56(±0.00)	62.33(±0.00)	62.82(±0.00)
	AEVC	68.75(±2.50)	81.01(±0.98)	74.44(±1.57)	61.15(±2.27)	60.40(±2.67)	60.25(±2.33)	61.94(±2.19)
	ETEAL	71.61(±0.00)	83.01(±0.00)	74.94(±0.00)	58.71(±0.00)	63.88(±0.00)	52.48(±0.00)	46.34(±0.00)
	S^2BGFMC	N/A	N/A	N/A	N/A	N/A	N/A	N/A
	HRFAL	**75.20(±0.00)**	**84.22(±0.00)**	**78.18(±0.00)**	**64.72(±0.00)**	**68.13(±0.00)**	**63.87(±0.00)**	64.64(±0.00)

Table 5: The comparison of running time (s) and time complexity for different approaches.

Methods	NGs	UCI	BDGP	Notting-Hill	Fashion	YTF10	YTF20	YTF50	Complexity
FDAGF	4.16	6.39	7.61	42.19	28.98	114.47	294.44	662.03	$O\left(\sum_{v=1}^{V}\sum_{r=1}^{R}(d_v m_r^2 + m_r^2 n + d_v m_r n)\right)$
Orth-NTF	60.70	277.54	98.83	327.91	276.20	N/A	N/A	N/A	$O(Vnmd + Vm^2k)$
MVSC-HFD	14.93	8.04	24.56	41.48	117.04	356.22	1129.12	4377.93	$O(n)$
OMVCDR	4.96	65.15	71.14	203.18	294.41	1369.80	3241.06	22137.62	$O\left(Td\sum_{p=1}^{m}d_p n + T\sum_{p=1}^{m}dd_p^2\right)$
AEVC	3.79	10.54	11.66	31.82	94.47	144.94	723.40	3023.13	$O(nm^3v + m^3v + nmdv + nmv)$
ETEAL	3.93	2.26	5.80	10.30	28.24	67.71	91.00	607.59	$O((Mnr^2\log(Mn) + M^2rn + d_h^3 + nd_h d_m + d_m d_h^2 + nrd_h + d_h r^2)t)$
S^2BGFMC	0.23	0.32	0.79	1.61	4.21	35.99	N/A	N/A	$O((nmk + nk^2 + V)T + ndmT_1 + ndm)$
HRFAL	**0.15**	**0.16**	**0.31**	**1.03**	**1.41**	**8.26**	**13.95**	**103.77**	$O((nmdV + m^2n + m^2nV + mn)t)$

consistent anchor graph for clustering, our method introduces an orthogonal diversity constraint to guarantee the disparity construction of the consistent anchor graph and the diversity anchor graphs, thus facilitating a more comprehensive exploration of both consistency and complementary information. In addition, the quality of the learned consistent information is improved by applying a Schatten p-norm to the consistent anchor graph to maintain it low-rank.

- The HRFAL model has the lowest running time on all datasets. As discussed in Section 3.8, the HRFAL model has a lower time complexity. This is because that the size of hypergraph is $m \times m$. By contrast, the size of the consistent anchor graph C and the diverse anchor graphs D^v both are $m \times n$, which greatly reduces the time complexity. Furthermore, as shown in Section 4.6, the HRFAL model can reach convergence quickly within 20 iterations, which also greatly reduces the time used. These results prove the effectiveness of our model in dealing with large-scale datasets.

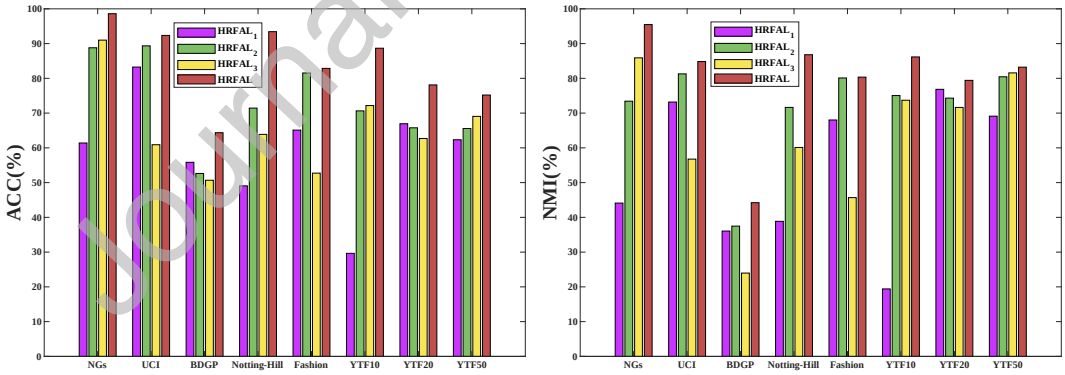

(a) ACC (b) NMI

Fig. 2: The ACC and NMI results of HRFAL_1, HRFAL_2, HRFAL_3, and HRFAL on eight datasets.

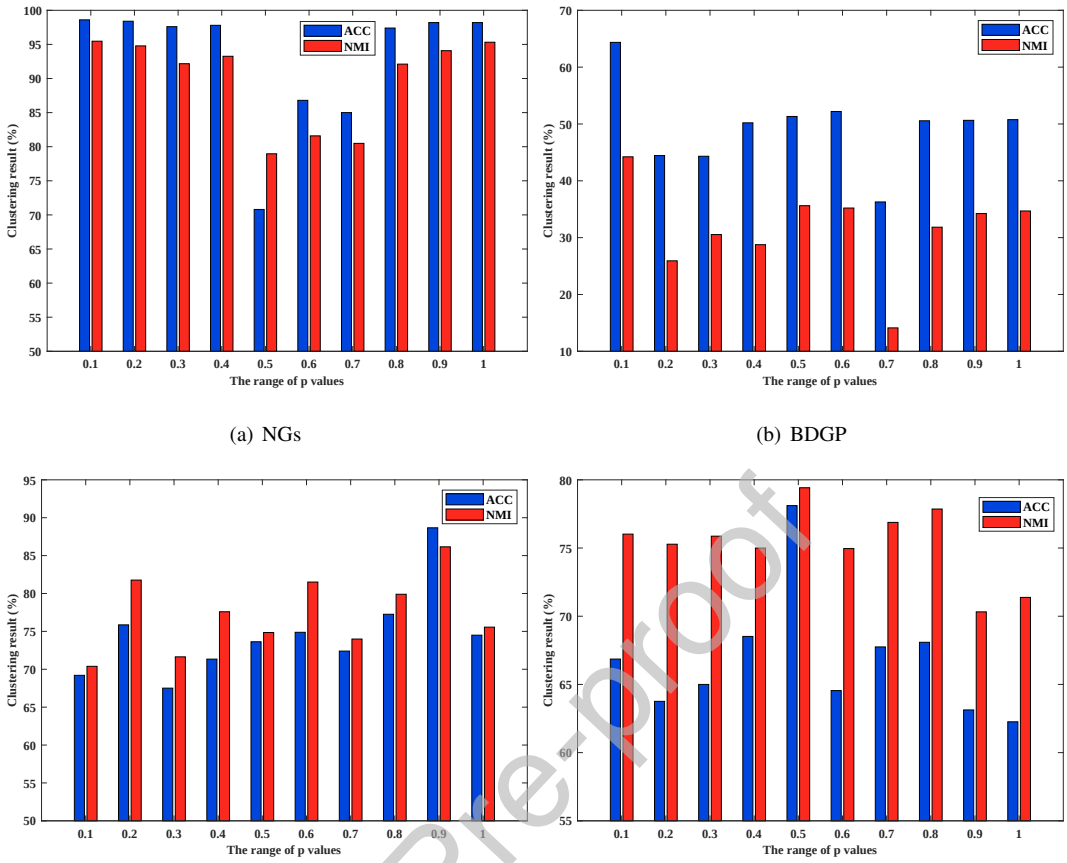

(a) NGs (b) BDGP

(c) YTF10 (d) YTF20

Fig. 3: The clustering performance of HRFAL with different values of p on different datasets.

4.4. Ablation study

In this section, we conduct two types of ablation studies: assessing the component validity of HRFAL and evaluating the influence of different values of p. In the first experiment, we focus on investigating the effects of hypergraph regularization on anchor points, the orthogonal diversity constraint between anchor graphs, and the Schatten p-norm for the consistent anchor graph. Three variants of HRFAL are obtained as follows:

- **HRFAL**$_1$: To verify the validity of the hypergraph regularization, we adjust $\alpha = 0$ in Eq. (11).
- **HRFAL**$_2$: To verify the validity of the orthogonal diversity constraint, we adjust $\beta = 0$ in Eq. (11).
- **HRFAL**$_3$: To verify the validity of the Schatten p-norm on the consistent anchor graph, we adjust $\gamma = 0$ in Eq. (11).

The results of ACC and NMI for HRFAL and three variants are presented in Fig. 2. It can be observed that HRFAL outperforms all three variants on all datasets. Thus, each component of the HRFAL model plays a key role in enhancing the efficacy of clustering.

To examine the impact of the values of p for our model, we adjust the parameter p in the range $[0.1, 0.2, \ldots, 0.9, 1]$, and conduct experiments on the NGs, BDGP, YTF10, and YTF20 datasets. The results are displayed in Fig. 3. As shown in the figure, the clustering results of HRFAL exhibit variability with different values of p. The best clustering results are achieved on all datasets when p ranges from 0.1 to 0.9, which are significantly better than those when $p = 1$. These results indicate that the Schatten p-norm can significantly enhance the quality of the consistent information for the consistent anchor graph.

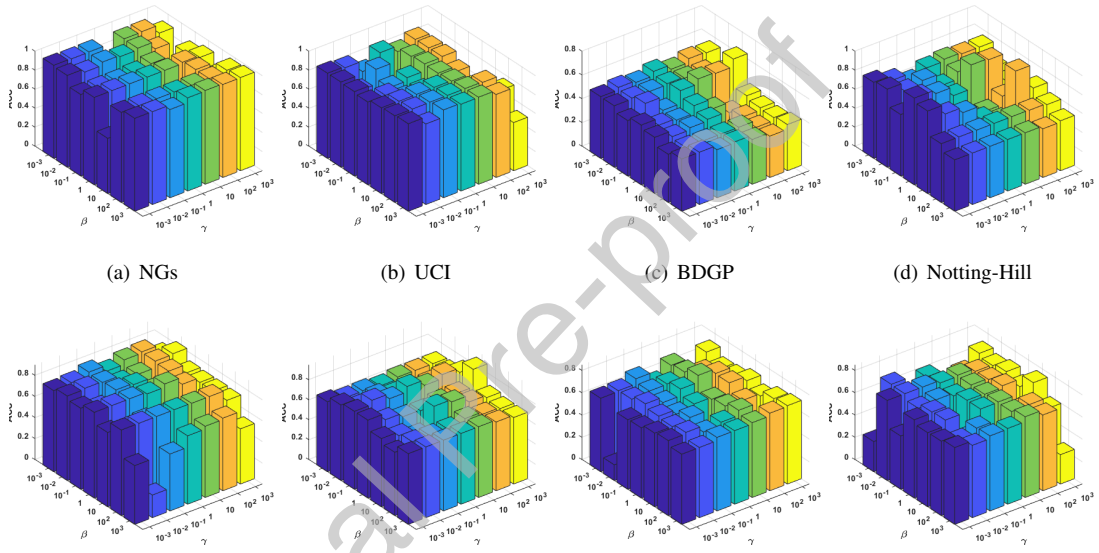

(a) NGs (b) UCI (c) BDGP (d) Notting-Hill

(e) Fashion (f) YTF10 (g) YTF20 (h) YTF50

Fig. 4: The ACC results of HRFAL versus β and γ on different datasets.

4.5. Parameter analysis

We perform experiments to examine the effects of α, β, γ, and the number of anchor points m in the HRFAL model. The values of α, β, and γ are tuned in $[10^{-3}, 10^{3}]$. In addition, the values of the anchor points m are $[2K, 3K, 4K, 5K, 6K, 7K]$. For α, β, and γ, we fix one parameter and adjust the other two ones to perform sensitivity experiments. The results of ACC on the eight datasets are shown in Figs. 4, 5, and 6. In addition, we investigate the clustering performance with different numbers of anchor points, and the results are shown in Fig. 7.

The parameter α controls the importance of the hypergraph regularization. As can be seen from the figures, the best results are obtained for ACC in all datasets when $10^{-2} \leq \alpha \leq 10^{2}$. The parameter β affects the role of the orthogonal diversity constraint. When $10^{-1} \leq \beta \leq 10^{3}$, the ACC results are the best in all datasets. The parameter γ affects the role of the Schatten p-norm on the HRFAL. When $1 \leq \gamma \leq 10^{3}$, the optimal ACC results are achieved on BDGP, NGs, Notting-Hill, Fashion, and YTF10. When $10^{-3} \leq \gamma \leq 10^{-1}$, the optimal ACC results are achieved on UCI, YTF20, and YTF50. As can be seen in Fig. 7, the number of anchor points affects the clustering results. When the number of anchor points is 3K, our method performed on NGs, BDGP, Fashion, YTF10, YTF20, and YTF50 can get better clustering performance.

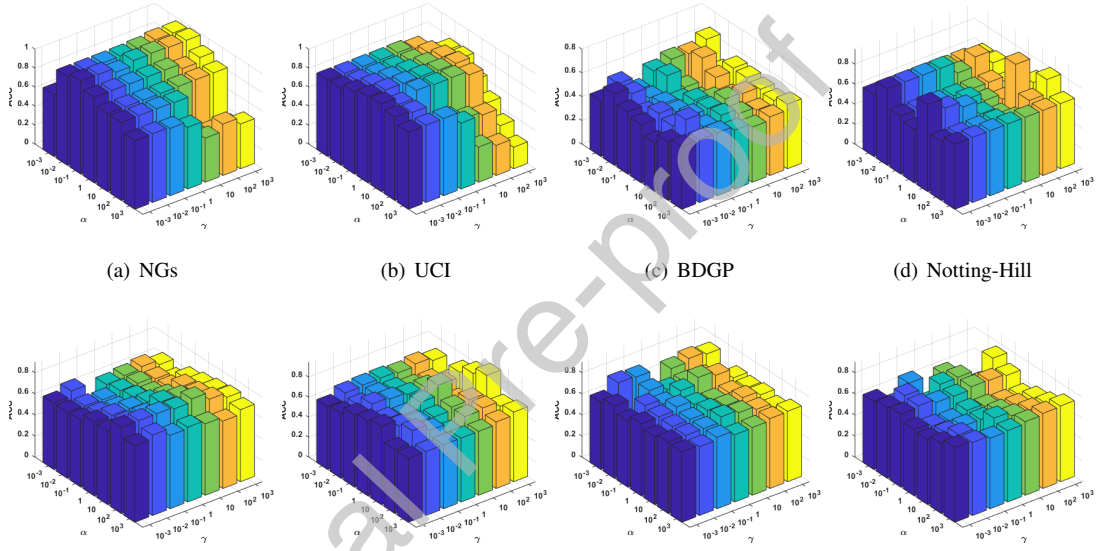

(a) NGs (b) UCI (c) BDGP (d) Notting-Hill

(e) Fashion (f) YTF10 (g) YTF20 (h) YTF50

Fig. 5: The ACC results of HRFAL versus α and γ on different datasets.

4.6. Convergence analysis

To investigate the convergence of HRFAL, the convergence curves of HRFAL are depicted in Fig. 8. As depicted in the figure, we can find that the objective curves decrease rapidly and reach convergence within 20 iterations.

4.7. Visualization

To better demonstrate the clustering performance of HRFAL, we take NGs (including 3 Views and 5 Classes), UCI (including 3 Views and 10 Classes), and Fashion (including 3 Views and 10 Classes) as

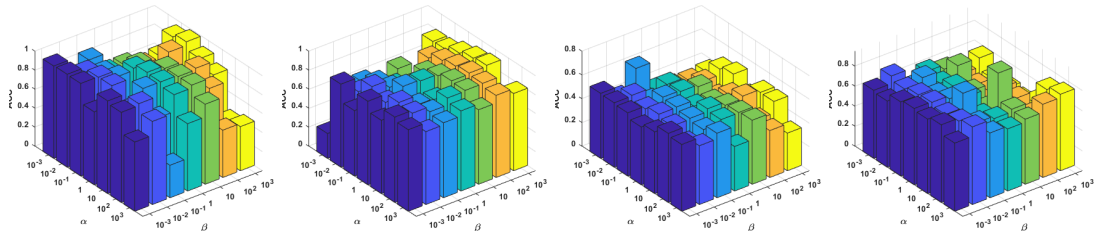

(a) NGs (b) UCI (c) BDGP (d) Notting-Hill

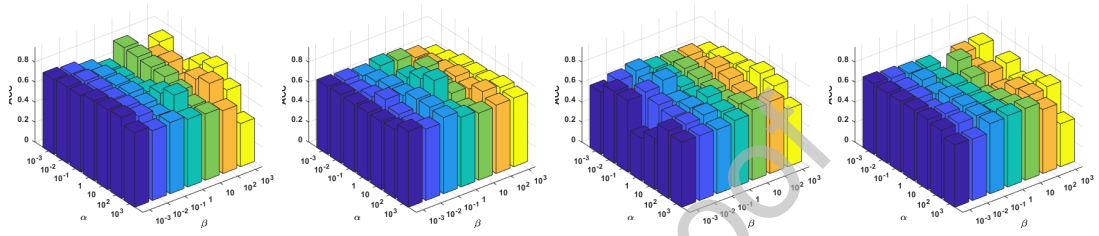

(e) Fashion (f) YTF10 (g) YTF20 (h) YTF50

Fig. 6: The ACC results of HRFAL versus α and β on different datasets.

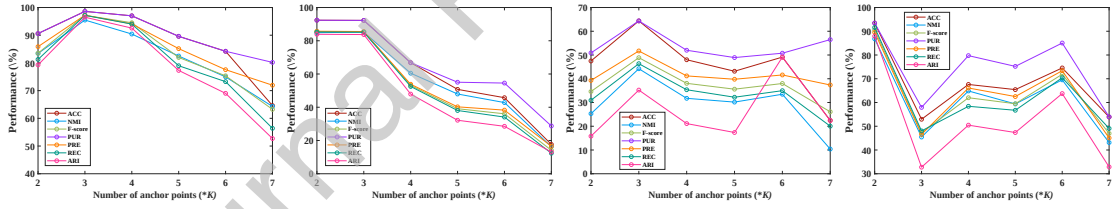

(a) NGs (b) UCI (c) BDGP (d) Notting-Hill

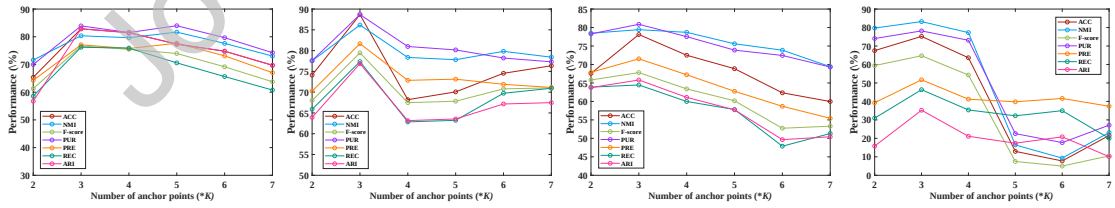

(e) Fashion (f) YTF10 (g) YTF20 (h) YTF50

Fig. 7: The results of HRFAL with different numbers of anchor points.

examples and present the corresponding visualization results via t-SNE [49]. The results are illustrated in Figs. 9, 10 and 11. From the three figures, we can observe that the processed data by HRFAL show a more compact clustering structure than the original data, which verifies that the HRFAL can achieve good clustering performance for multi-view data.

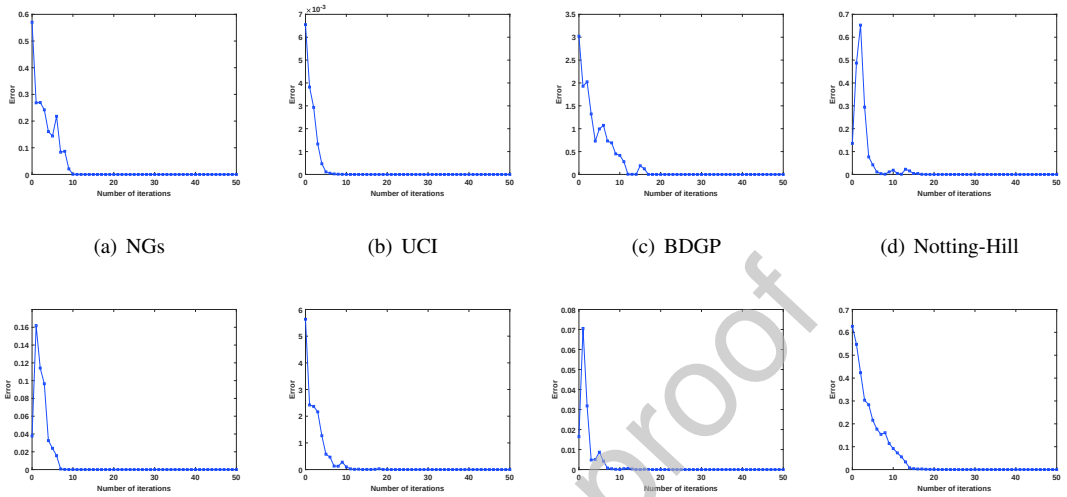

(a) NGs (b) UCI (c) BDGP (d) Notting-Hill

(e) Fashion (f) YTF10 (g) YTF20 (h) YTF50

Fig. 8: The convergence curves of HRFAL.

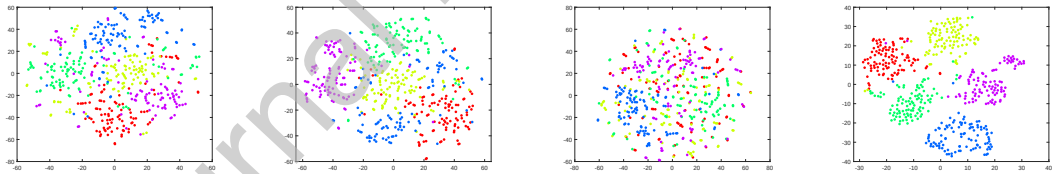

(a) View 1 (b) View 2 (c) View 3 (d) The clustering results

Fig. 9: Visualization of each view of the NGs dataset and the final clustering results.

5. Conclusions

In this paper, we develop a novel anchor-based MVSC method called HRFAL. The core idea is to apply hypergraph regularization to the anchor points to explore the relationship between the anchor points. Then, we apply the orthogonal diversity constraint to the learned consistent and diverse anchor graphs to better utilize the consistent and complementary information. Furthermore, the Schatten p-norm is

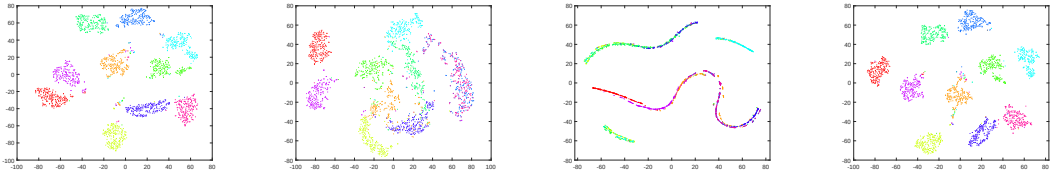

(a) View 1 (b) View 2 (c) View 3 (d) The clustering results

Fig. 10: Visualization of each view of the UCI dataset and the final clustering results.

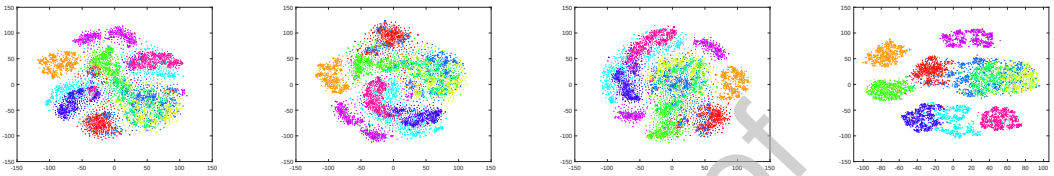

(a) View 1 (b) View 2 (c) View 3 (d) The clustering results

Fig. 11: Visualization of each view of the Fashion dataset and the final clustering results.

introduced to better learn the consistent information. Experimental results on eight real-world datasets validate the effectiveness and superiority of the proposed HRFAL method.

It is worth pointing out that our method does not fully consider the noise and irrelevant information. Thus, in the future, we would like to concentrate on learning consistent and diverse anchor graphs in the embedding space to boost enhance the clustering performance.

Acknowledgment

This study was funded by the Natural Science Foundation of Shandong Province under Grant ZR2023MF063, and the Graduate Innovation Foundation of Yantai University (GIFYTU).

References

[1] D. J. Trosten, S. Løkse, R. Jenssen, M. C. Kampffmeyer, On the effects of self-supervision and contrastive alignment in deep multi-view clustering, in: Proceedings of the IEEE/CVF Conference on Computer Vision and Pattern Recognition, 2023, pp. 23976–23985.

[2] M.-S. Chen, L. Huang, C.-D. Wang, D. Huang, Multi-view clustering in latent embedding space, in: Proceedings of the AAAI Conference on Artificial Intelligence, 2020, pp. 3513–3520.

[3] G. A. Khan, J. Khan, T. Anwar, Z. Ashraf, M. H. Javed, B. Diallo, Weighted concept factorization based incomplete multi-view clustering, IEEE Transactions on Artificial Intelligence 5 (11) (2024) 5699–5708.

[4] Z. Kou12, J. Wang12, Y. Jia12, X. Geng, Exploiting multi-label correlation in label distribution learning (2024) 4326–4334.

[5] H. Lu, H. Xu, Q. Wang, Q. Gao, M. Yang, X. Gao, Efficient multi-view-means for image clustering, IEEE Transactions on Image Processing 33 (2023) 273–284.

[6] G. Chao, S. Sun, J. Bi, A survey on multiview clustering, IEEE Transactions on Artificial Intelligence 2 (2) (2021) 146–168.

[7] Z. Kou, J. Wang, Y. Jia, B. Liu, X. Geng, Instance-dependent inaccurate label distribution learning, IEEE Transactions on Neural Networks and Learning Systems 36 (1) (2025) 1425–1437.

[8] Y. Cheng, P. Song, Incomplete multi-view clustering via confidence graph completion based tensor decomposition, Expert Systems with Applications 258 (2024) 125151.

[9] W. Zhao, Q. Li, H. Xu, Q. Gao, Q. Wang, X. Gao, Anchor graph-based feature selection for one-step multi-view clustering, IEEE Transactions on Multimedia (2024) 7413 – 7425.

[10] S. Luo, C. Zhang, W. Zhang, X. Cao, Consistent and specific multi-view subspace clustering, in: Proceedings of the AAAI Conference on Artificial Intelligence, Vol. 32, 2018, pp. 3730–3737.

[11] P. Zhang, X. Liu, J. Xiong, S. Zhou, W. Zhao, E. Zhu, Z. Cai, Consensus one-step multi-view subspace clustering, IEEE Transactions on Knowledge and Data Engineering 34 (10) (2022) 4676–4689.

[12] X. Si, Q. Yin, X. Zhao, L. Yao, Consistent and diverse multi-view subspace clustering with structure constraint, Pattern Recognition 121 (2022) 108196.

[13] Q. Zheng, J. Zhu, Z. Li, Z. Tian, C. Li, Comprehensive multi-view representation learning, Information Fusion 89 (2023) 198–209.

[14] J. Wang, B. Wu, Z. Ren, Y. Zhou, Decomposed deep multi-view subspace clustering with self-labeling supervision, Information Sciences 653 (2024) 119798.

[15] J. Wang, Z. Kou, Y. Jia, J. Lv, X. Geng, Label distribution learning by exploiting fuzzy label correlation, IEEE Transactions on Neural Networks and Learning Systems 36 (5) (2025) 8979–8990.

[16] Z. Kou, J. Wang, Y. Jia, X. Geng, Inaccurate label distribution learning, IEEE Transactions on Circuits and Systems for Video Technology 34 (10) (2024) 10237–10249.

[17] J. Lao, D. Huang, C. D. Wang, J. H. Lai, Towards scalable multi-view clustering via joint learning of many bipartite graphs, IEEE Transactions on Big Data 10 (1) (2024) 77–91.

[18] P. Zhang, S. Wang, L. Li, C. Zhang, X. Liu, E. Zhu, Z. Liu, L. Zhou, L. Luo, Let the data choose: Flexible and diverse anchor graph fusion for scalable multi-view clustering, in: Proceedings of the AAAI Conference on Artificial Intelligence, Vol. 37, 2023, pp. 11262–11269.

[19] Q. Ou, S. Wang, P. Zhang, S. Zhou, E. Zhu, Anchor-based multi-view subspace clustering with hierarchical feature descent, Information Fusion 106 (2024) 102225.

[20] S. Wang, X. Liu, S. Liu, W. Tu, E. Zhu, Scalable and structural multi-view graph clustering with adaptive anchor fusion, IEEE Transactions on Image Processing (2024) 4627 – 4639.

[21] S. Liu, K. Liang, Z. Dong, S. Wang, X. Yang, S. Zhou, E. Zhu, X. Liu, Learn from view correlation: An anchor enhancement strategy for multi-view clustering, in: Proceedings of the IEEE/CVF Conference on Computer Vision and Pattern Recognition, 2024, pp. 26151–26161.

[22] M.-S. Chen, C.-D. Wang, D. Huang, J.-H. Lai, S. Y. Philip, Concept factorization based multiview clustering for large-scale data, IEEE Transactions on Knowledge and Data Engineering 36 (11) (2024) 5784 – 5796.

[23] X. Wang, X. Guo, Z. Lei, C. Zhang, S. Z. Li, Exclusivity-consistency regularized multi-view subspace clustering, in: Proceedings of the IEEE Conference on Computer Vision and Pattern Recognition, 2017, pp. 923–931.

[24] Q. Zheng, J. Zhu, Z. Tian, Z. Li, S. Pang, X. Jia, Constrained bilinear factorization multi-view subspace clustering, Knowledge-Based Systems 194 (2020) 105514.

[25] Z. Li, C. Tang, X. Zheng, X. Liu, W. Zhang, E. Zhu, High-order correlation preserved incomplete multi-view subspace clustering, IEEE Transactions on Image Processing 31 (2022) 2067–2080.

[26] G. Y. Zhang, D. Huang, C. D. Wang, Facilitated low-rank multi-view subspace clustering, Knowledge-Based Systems 260 (2023) 110141.

[27] S. Peng, J. Yin, Z. Yang, B. Chen, Z. Lin, Multiview clustering via hypergraph induced semi-supervised symmetric nonnegative matrix factorization, IEEE Transactions on Circuits and Systems for Video Technology 33 (10) (2023) 5510–5524.

[28] A. Dong, Z. Wu, H. Zhang, Multi-view subspace clustering based on adaptive search, Knowledge-Based Systems 289 (2024) 111553.

[29] J. Bian, X. Xie, C. D. Wang, L. Yang, J. H. Lai, F. Nie, Angular reconstructive discrete embedding with fusion similarity for multi-view clustering, IEEE Transactions on Knowledge and Data Engineering 37 (1) (2025) 45–59.

[30] W. Xia, Q. Gao, Q. Wang, X. Gao, C. Ding, D. Tao, Tensorized bipartite graph learning for multi-view clustering, IEEE Transactions on Pattern Analysis and Machine Intelligence 45 (4) (2023) 5187–5202.

[31] S. Liu, S. Wang, P. Zhang, K. Xu, X. Liu, C. Zhang, F. Gao, Efficient one-pass multi-view subspace clustering with consensus anchors, in: Proceedings of the AAAI Conference on Artificial Intelligence, Vol. 36, 2022, pp. 7576–7584.

[32] Y. Zhang, G. Jiang, Z. Cai, Y. Zhou, Bipartite graph-based projected clustering with local region guidance for hyperspectral imagery, IEEE Transactions on Multimedia 26 (2024).

[33] S. Liu, Q. Liao, S. Wang, X. Liu, E. Zhu, Robust and consistent anchor graph learning for multi-view clustering, IEEE Transactions on Knowledge and Data Engineering 36 (8) (2024) 4207–4219.

[34] C. Zhang, X. Jia, Z. Li, C. Chen, H. Li, Learning cluster-wise anchors for multi-view clustering, in: Proceedings of the AAAI conference on artificial intelligence, Vol. 38, 2024, pp. 16696–16704.

[35] J. Wu, B. Yang, S. Yang, X. Zhang, B. Chen, Scalable sparse bipartite graph factorization for multi-view clustering, Expert Systems with Applications 267 (2025) 126192.

[36] Q. Dai, Y. Gao, Hypergraph computation, Springer Nature, 2023.

[37] Y. Luo, H. Chen, T. Yin, S.-J. Horng, T. Li, Dual hypergraphs with feature weighted and latent space learning for the diagnosis of Alzheimer's disease, Information Fusion 112 (2024) 102546.

[38] Y. Cheng, P. Song, J. Mu, Y. Yu, W. Zheng, Comprehensive multi-view self-representations for clustering, Expert Systems with Applications 251 (2024) 124103.

[39] W. Lan, T. Yang, Q. Chen, S. Zhang, Y. Dong, H. Zhou, Y. Pan, Multiview subspace clustering via low-rank symmetric affinity graph, IEEE Transactions on Neural Networks and Learning Systems 35 (8) (2024) 11382 – 11395.

[40] G. Du, P. Song, Y. Cheng, Z. Liu, Y. Yu, W. Zheng, Weighted tensor-based consistent anchor graph learning for multi-view clustering, Neurocomputing 620 (2025) 129253.

[41] C. Zhang, H. Li, W. Lv, Z. Huang, Y. Gao, C. Chen, Enhanced tensor low-rank and sparse representation recovery for incomplete multi-view clustering, in: Proceedings of the AAAI Conference on Artificial Intelligence, Vol. 37, 2023, pp. 11174–11182.

[42] C. Zhang, D. Xu, X. Jia, C. Chen, H. Li, Continual multi-view clustering with consistent anchor guidance, in: Proc. 33rd Int. Joint Conf. Artif. Intell., 2024, pp. 5434–5442.

[43] D. Huang, C. D. Wang, J. H. Lai, Fast multi-view clustering via ensembles: Towards scalability, superiority, and simplicity, IEEE Transactions on Knowledge and Data Engineering 35 (11) (2023) 11388–11402.

[44] Y. Qin, N. Pu, H. Wu, EDMC: efficient multi-view clustering via cluster and instance space learning, IEEE Transactions on Multimedia 26 (2023) 5273–5283.

[45] D. Cai, Litekmeans: the fastest matlab implementation of kmeans, Software available at: http://www.zjucadcg.cn/dengcai/Data/Clustering.html 311 (2011).

[46] J. Li, Q. Gao, Q. Wang, M. Yang, W. Xia, Orthogonal non-negative tensor factorization based multi-view clustering, Advances in Neural Information Processing Systems 36 (2023) 18186–18202.

[47] X. Wan, J. Liu, X. Gan, X. Liu, S. Wang, Y. Wen, T. Wan, E. Zhu, One-step multi-view clustering with diverse representation, IEEE Transactions on Neural Networks and Learning Systems 36 (3) (2025) 5774 – 5786.

[48] B. Yang, P. Song, Y. Cheng, S. Zhou, Z. Liu, Enhanced tensor based embedding anchor learning for multi-view clustering, Information Sciences 690 (2025) 121532.

[49] L. Van der Maaten, G. Hinton, Visualizing data using t-SNE, Journal of machine learning research 9 (11) (2008).

Declaration of interests

The authors declare that they have no known competing financial interests or personal relationships that could have appeared to influence the work reported in this paper.

The authors declare the following financial interests/personal relationships which may be considered as potential competing interests: